

Advancements in implantable temperature sensors: Materials, mechanisms, and biological applications

Zhuofan Yang¹, Hongcheng Song^{2,†}, and He Ding^{1,†}

¹Beijing Engineering Research Center of Mixed Reality and Advanced Display, School of Optics and Photonics, Beijing Institute of Technology, Beijing 100081, China

²Department of Urology, Beijing Children's Hospital, Capital Medical University, National Center for Children's Health, Beijing 100045, China

Abstract: Implantable temperature sensors are revolutionizing physiological monitoring and playing a crucial role in diagnostics, therapeutics, and life sciences research. This review classifies the materials used in these sensors into three categories: metal-based, inorganic semiconductor, and organic semiconductor materials. Metal-based materials are widely used in medical and industrial applications due to their linearity, stability, and reliability. Inorganic semiconductors provide rapid response times and high miniaturization potential, making them promising for biomedical and environmental monitoring. Organic semiconductors offer high sensitivity and ease of processing, enabling the development of flexible and stretchable sensors. This review analyzes recent studies for each material type, covering design principles, performance characteristics, and applications, highlighting key advantages and challenges regarding miniaturization, sensitivity, response time, and biocompatibility. Furthermore, critical performance parameters of implantable temperature sensors based on different material types are summarized, providing valuable references for future sensor design and optimization. The future development of implantable temperature sensors is discussed, focusing on improving biocompatibility, long-term stability, and multifunctional integration. These advancements are expected to expand the application potential of implantable sensors in telemedicine and dynamic physiological monitoring.

Key words: implantable; temperature sensors; biological applications; flexible electronics

Citation: Z F Yang, H C Song, and H Ding, Advancements in implantable temperature sensors: Materials, mechanisms, and biological applications[J]. *J. Semicond.*, 2025, 46(1), 011609. <https://doi.org/10.1088/1674-4926/24100003>

1. Introduction

Over the past few decades, the field of implantable medical devices has made tremendous progress, with implantable temperature sensors fundamentally changing how we monitor and understand physiological states. These miniaturized, high-precision sensors can be directly implanted in the body to provide real-time, continuous temperature data, opening new prospects for medical diagnosis, treatment, and life science research^[1, 2]. Body temperature, one of the most important physiological parameters, has always been a core indicator in medical diagnosis and health monitoring^[3–6]. Conventional body temperature measurements, such as oral thermometers or handheld temperature guns, are straightforward and user-friendly. However, they can offer intermittent surface temperature data and might be influenced by the ambient temperature^[7]. In contrast, implantable temperature sensors continuously monitor temperature changes in specific body parts, providing doctors and researchers with more comprehensive and accurate information^[8–11]. The application range of implantable temperature sensors is broad. In clinical medicine, they can be used for early disease diagnosis, organ temperature monitoring during surgery, and chronic dis-

ease management. These sensors provide valuable neuroscience, drug development, and tissue engineering tools in life science research. Furthermore, in emerging fields such as remote medical care and environmental health monitoring, implantable temperature sensors show great potential^[8, 9, 12].

Although implantable and wearable temperature sensors open new possibilities for personalized medicine and real-time health monitoring, they face more significant challenges and higher technical requirements than wearable sensors^[13–16]. Since it is difficult to repair or replace after implantation, the design of these sensors must fully consider the complexity of the human internal environment to ensure long-term stable performance and reliable operation after implantation^[17]. Compared to wearable sensors, implantable sensors face additional challenges, such as avoiding immune responses or tissue inflammation, ensuring durability in the presence of bodily fluids, and managing power consumption to operate for extended periods without frequent recharging or battery replacement. These challenges highlight that implantable temperature sensors face more technical hurdles than wearable sensors in their research and development process. Researchers are exploring and optimizing various materials to address these challenges. Three representative categories of materials that have shown outstanding performance in developing implantable temperature sensors are metal-based, inorganic, and organic semiconductor materials. Each of these materials has unique characteristics and plays a crucial role in meeting the stringent requirements of

Correspondence to: H C Song, songhch1975@126.com; H Ding, heding@bit.edu.cn

Received 4 OCTOBER 2024; Revised 29 OCTOBER 2024.

©2025 Chinese Institute of Electronics. All rights, including for text and data mining, AI training, and similar technologies, are reserved.

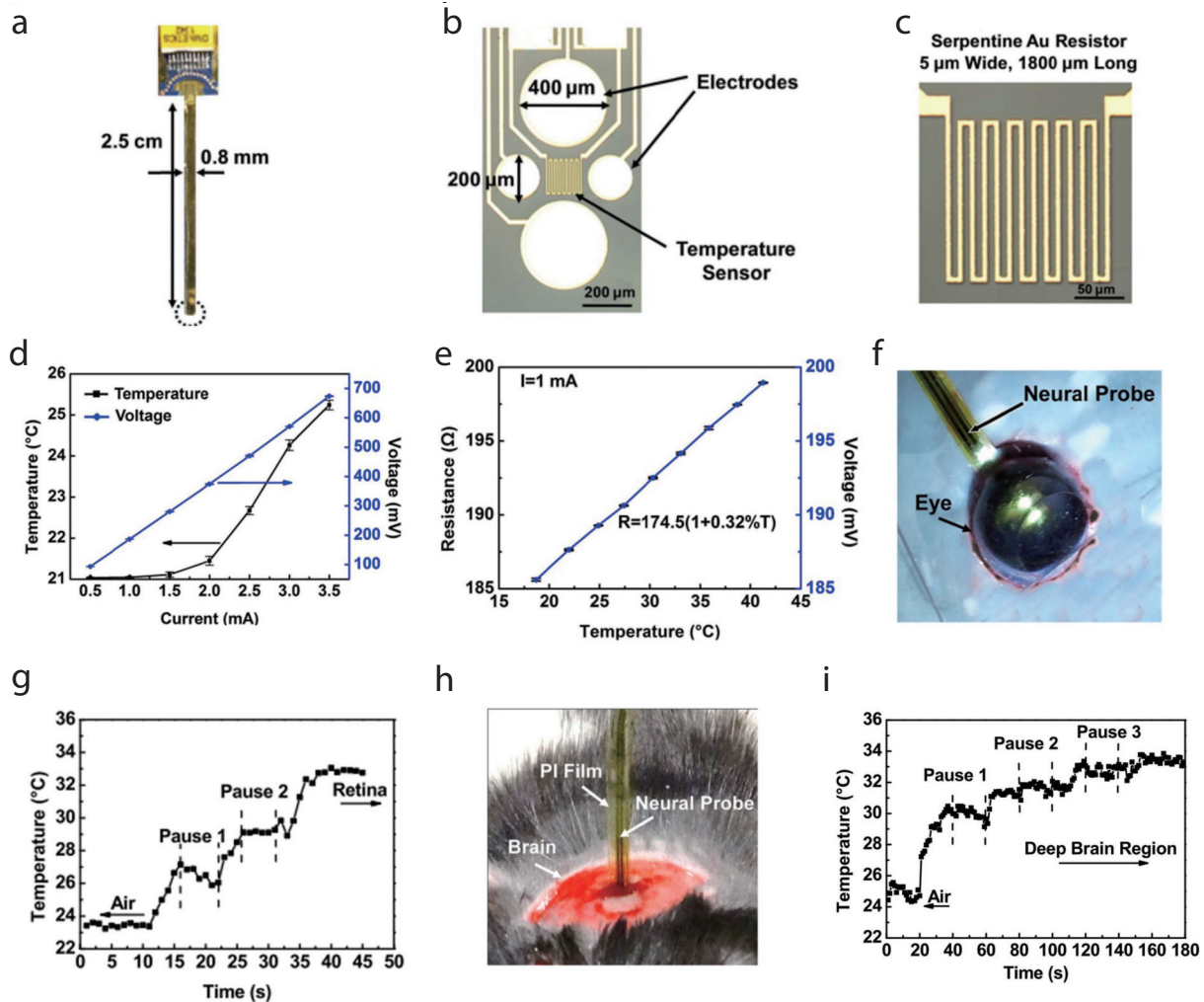


Fig. 1. (Color online) Implantable, biocompatible Au resistive temperature sensors. (a) A flexible implantable neural probe on a polyimide (PI) substrate, attached to printed circuit boards (PCBs) with connectors. (b) A detailed view of the probe tip, containing electrodes and temperature sensors. (c) Temperature sensor made of a serpentine gold wire 5 μm wide and 1800 μm long. (d) The temperature and voltage responses of the temperature sensor when a 1 mA current is applied. (e) The resistive temperature sensor exhibits a linear relationship between resistance and voltage under a 1 mA current, with a temperature coefficient of 0.32%. (f) Optical image of the neural probe implanted in the retina, monitoring temperature changes during insertion. (g) Temperature changes during probe implantation in the retina. (h) Optical image of the neural probe implanted in the deep brain region. (i) Temperature changes during probe implantation were monitored in the deep brain. Reproduced with permission from Ref. [25]. Copyright (2017) IEEE.

implantable devices, driving advancements in related technologies, and laying a foundation for future biomedical sensing technology.

2. Metal-based implantable temperature sensor

Metal-based temperature sensors are among the earliest developed implantable temperature sensors, utilizing the temperature-dependent electrical resistance of metallic materials for measurement. They are recognized for their linearity, stability, and reliability in medical^[18], industry^[19, 20], and other applications^[21]. The core component is the temperature-sensitive element, typically made from pure metals or specific alloys. These materials exhibit a linear resistance-temperature relationship within a defined range^[22], enabling accurate measurements. Common metallic materials include platinum (Pt), gold (Au), nickel (Ni), and manganese (Mn). Although noble metals like Pt and Au have high prices, the simple structure of these sensors and the relatively mature manufacturing process result in higher feasibility and medium production costs.

Recent advancements in micro- and nano-fabrication technologies have improved the miniaturization and integration of these sensors, expanding their use in implantable medical devices^[23, 24]. However, the biocompatibility and flexibility of metallic materials remain challenges, prompting research into novel material combinations and structural designs to enhance performance.

Wang *et al.* have developed flexible polyimide-based neural probes integrated with metal-resistive temperature sensors (Fig. 1(a)) to monitor temperature changes during neural probe implantation and stimulation in the retina and deep brain regions^[25]. The temperature sensor is located at the tip of the probe, adjacent to the electrical stimulation site, which consists of serpentine gold (Au) lines measuring 5 μm wide and 1800 μm long, as illustrated in Figs. 1(b) and 1(c). Polyimide (PI) film with a thickness of 1 μm encapsulates the temperature sensor, allowing it to monitor tissue temperature with a thermal conductivity of 0.2 W·(m·K)⁻¹ while protecting the Au resistor from degradation due to direct tissue contact.

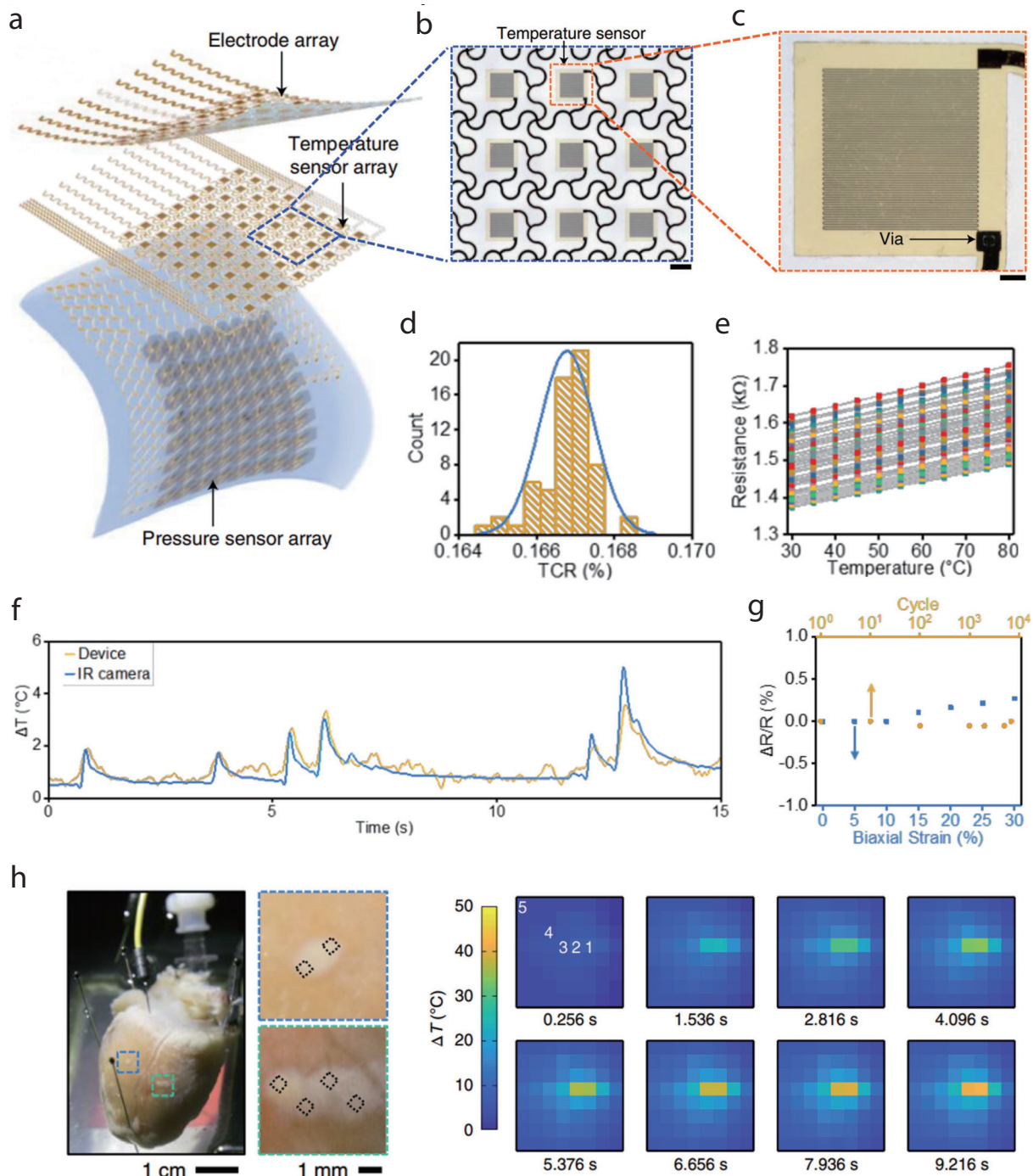


Fig. 2. (Color online) Implantable, biocompatible soft multilayer electronic arrays for the functional temperature sensor. (a) Schematic illustration of the multimodal, multiplexed soft sensors in a multilayer configuration, including 8×8 electrodes for radiofrequency ablation (RFA) and irreversible electroporation (IRE), temperature sensors for precision thermography, and pressure sensors for measuring forces associated with soft-tissue contact. (b) Detailed view of the temperature sensor array in a planar format. (c) Temperature sensor made of a thin Au metal wire with a thickness of 100 nm and a width of $4\text{ }\mu\text{m}$, configured as a resistance element. (d) Histogram and Gaussian lineshape fitting of the temperature coefficient of resistance (TCR) values for the temperature sensors. (e) Resistance measurements from the sixty-four temperature sensors at temperatures ranging from 30 to $80\text{ }^{\circ}\text{C}$. (f) Comparison of results from the infrared camera and the stretchable temperature sensor array, with the circuit properly grounded to eliminate crosstalk. (g) Fractional change of resistance of a temperature sensor under cyclic 20% uniaxial stretching (orange points) and different biaxial strains (blue points). (h) Spatiotemporal temperature mapping measured by the temperature sensor array during bipolar RFA on a rabbit heart. Reproduced with permission from Ref. [30]. Copyright (2020) Nature Publishing Group.

This arrangement makes the temperature sensor miniaturized, biocompatible, and tightly integrated with the electrodes, facilitating accurate temperature distribution measurement within the tissue^[26, 27]. Fig. 1(d) shows experiments with a maximum self-induced temperature increase of $4.2\text{ }^{\circ}\text{C}$ when the direct current (DC) was adjusted from 0.2 to 3.5 mA .

However, with the Au-based resistor temperature sensor operating at only 1 mA DC , the resultant temperature rise is less than $0.05\text{ }^{\circ}\text{C}$, indicating a negligible self-heating effect. Fig. 1(e) demonstrates a temperature coefficient of 0.32% and maintains good linearity for the Au-based temperature sensor, ensuring accurate and biocompatible temperature

monitoring. Figs. 1(f)–1(i) present *in vivo* experiments where the sensor successfully detected temperature changes in the retina (Figs. 1(f) and 1(g)) and brain tissue (Figs. 1(h) and 1(i)) in live animal models. The implantation process was paused several times to demonstrate stability and reliability in dynamic physiological environments. The results indicate that the sensor successfully monitored temperature changes in the retina and deep brain regions during electrical stimulation in initial *in vivo* experiments, providing valuable data for further investigation into the thermal effects of electrical stimulation on tissue.

Different from single-point temperature recording, array-based temperature sensors capture temperature distributions across a wide area, enabling high-resolution spatiotemporal mapping and providing insights into temperature gradients across tissue surfaces^[28, 29]. Han *et al.* developed a catheter-integrated soft multilayer electronic array designed for minimally invasive cardiac surgery, focusing on the array-based temperature recording system^[30]. This array is arranged in an 8 × 8 grid, as shown in Fig. 2(a). It utilizes stretchable interconnects, multilayer construction, and advanced semiconductor manufacturing techniques to achieve high-density and multimodal functionality. Figs. 2(b) and 2(c) display the planar format of the temperature sensors, where each sensor consists of thin gold (Au) traces embedded in a polyimide (PI) layer, functioning as resistive elements whose resistance changes in response to temperature fluctuations. To comprehensively understand the performance characteristics of the sensor, Figs. 2(d) and 2(e) collectively present the performance evaluation of the temperature sensor. Fig. 2(d) shows the histogram of the temperature resistance coefficient (TCR) of the sensor array. The result fitting curve for analysis shows a good Gaussian distribution, indicating that the TCR values are concentrated in a relatively narrow range and the temperature response performance is uniform. Fig. 2(e) demonstrates the resistance changes of the 8 × 8 temperature sensor array over a temperature range of 30 to 80 °C, indicating a centralized and uniform TCR distribution with excellent linear response characteristics. Fig. 2(f) compares the measurement results of an infrared camera with those of the flexible temperature sensor array after proper grounding to eliminate crosstalk. The results show that after interference correction, the measurements from the flexible sensor array align closely with those from the infrared camera, verifying the accuracy and reliability of the flexible sensor in practical applications. To evaluate long-term stability, the researchers presented the rate of resistance change of the temperature sensor under different strain conditions in Fig. 2(g). The temperature sensor maintained relatively stable resistance changes under periodic uniaxial tensile and biaxial strains, demonstrating excellent mechanical stability. This indicates the sensor reliably preserves its temperature-sensing performance under dynamic stretching and deformation environments. Fig. 2(h) illustrates the performance of this multifunctional flexible electronic array on a rabbit heart, where spatial and temporal mapping of tissue surface temperature distribution was achieved during radiofrequency ablation (RFA). This flexible array sensor system shows promise for enhancing the performance and functionality of medical devices, potentially opening new

avenues for clinical diagnosis and treatment. This technology is expected to provide novel solutions for more precise and intelligent medical procedures through continuous optimization of design and manufacturing processes, sensor performance and reliability improvements, and deep integration with surgical instruments^[31–33].

Additionally, optoelectronic devices have biosensing^[34], medical imaging^[35], and optogenetics^[36] applications. Monitoring temperature elevations in tissues near light sources is crucial to prevent damage from localized overheating. However, conventional temperature sensors often interfere with optical signals and reduce the efficiency of optoelectronic devices due to their opacity^[37]. Cui *et al.* have developed a transparent temperature sensor based on Mn-Co-Ni-O (MCN) nanofilms^[38], and Fig. 3(a) shows the sensor design in detail, highlighting the thin and transparent form of the sensor. This sensor can be directly integrated into optical probes or micro-LEDs, and its transparency ensures that it does not impede light transmission. Fig. 3(b) shows the sandwich structure of encapsulation layer — sensitive layer — encapsulation layer, in which SiO₂ is used to provide mechanical support and interference resistance. The MCN-sensitive layer is about 100 nm thick, with water-soluble germanium oxide used as a sacrificial layer to prepare self-supporting sensor films. Figs. 3(c) and 3(d) demonstrate the high-temperature sensitivity of the sensor, with a temperature coefficient of resistance (TCR) of 4% °C⁻¹, exhibiting an excellent linear response and accurately detecting small temperature changes down to 0.03 °C. This indicates outstanding high-temperature resolution, ensuring accurate reflection of resistance changes with temperature variations. Fig. 3(e) explores the transient temperature response characteristics, and the experimental results reveal a response time of 224 ms as the detection temperature increases from 25 to 70 °C, indicating a high response speed. Figs. 3(f) and 3(g) show schematic and optical images of the integrated probe, the sensor can be integrated directly above the LED with little obstruction to the light due to its excellent transparency. Fig. 3(h) further demonstrates that the LED light can penetrate through the temperature sensor, with only a slight decrease in the light intensity. Fig. 3(i) shows the curve measured by the integrated MCN transparent temperature sensor is consistent with the calibrated infrared measurement curve, with an error of less than 1%, demonstrated the sensor's capability to accurately capture the surface temperature rise of the LED. Comparative analysis of the control group (Fig. 3(j)) and the tissue sections surrounding the implant after 21 days (Fig. 3(k)) demonstrates excellent biocompatibility. This MCN transparent temperature sensor exhibits high sensitivity, excellent biocompatibility, and robust interference resistance, indicating broad application prospects in optogenetics, biomedicine, and optoelectronics. Future work may focus on optimizing the sensor to enhance its utility in biomedical applications, thereby supporting the development of implantable bioelectronic devices and related fields.

3. Inorganic semiconductor-based implantable temperature sensor

Inorganic semiconductor materials are gaining attention in implantable temperature sensors, emerging as a rapidly

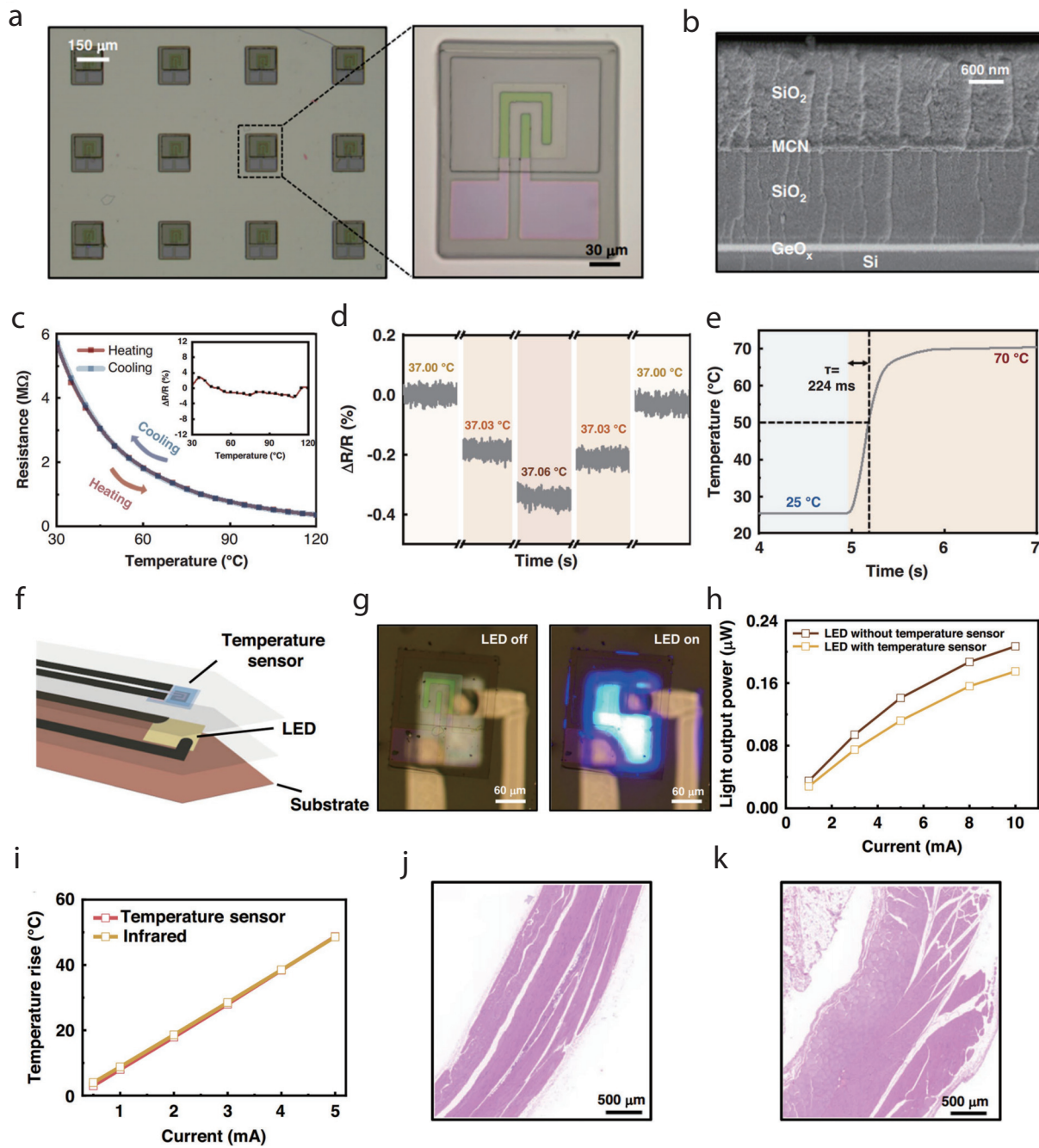


Fig. 3. (Color online) Implantable, biocompatible, transparent temperature sensor based on a Mn-Co-Ni-O nanofilm. (a) Optical image of the Mn-Co-Ni-O nanofilm temperature sensors on a Si substrate. (b) Scanning electron microscopy (SEM) image of a sandwich-structured thin-film temperature sensor on a Si substrate with a total thickness of approximately 4.1 μm . (c) Resistance variation with temperature for the Mn-Co-Ni-O (MCN) transparent temperature sensor. (d) Resolution test for the freestanding MCN transparent temperature sensor, demonstrating the ability to detect a small temperature change of 0.03 °C. (e) Response time of the MCN transparent temperature sensor is 224 ms when transitioning from 25 to 70 °C. (f) Schematic illustrations of the microscale LED probe integrated with the MCN transparent temperature sensor. (g) Optical image of the microscale LED probe integrated with the MCN transparent temperature sensor, showing blue light from the LED penetrating through the sensor. (h) Luminous power of LEDs with and without integrated temperature sensors as a function of input current. (i) Measurement of the increase in temperature of the LED surface under different injection currents by the MCN transparent temperature sensor and an infrared camera. (j) Hematoxylin and eosin (H&E)-stained histological section image of the control group, showing the back region of a rat without implantation. (k) Histological section image of the tissue surrounding the sensor after 21 days of implantation in the back region of a rat. Reproduced with permission from Ref. [38]. Copyright (2024) Nature Publishing Group.

developing research direction^[39, 40]. The growth and fabrication of these inorganic semiconductor-based sensors typically utilize advanced and complex microfabrication techniques, making them more difficult to produce and resulting in higher manufacturing costs compared to other sensor types. They leverage the temperature-dependent electrical or

optical properties of semiconductor materials for accurate temperature measurement. They offer advantages such as high sensitivity, rapid response, and significant miniaturization, demonstrating potential for biomedical and environmental monitoring applications. Silicon (Si) is one of the most widely used inorganic semiconductor materials, serving as a founda-

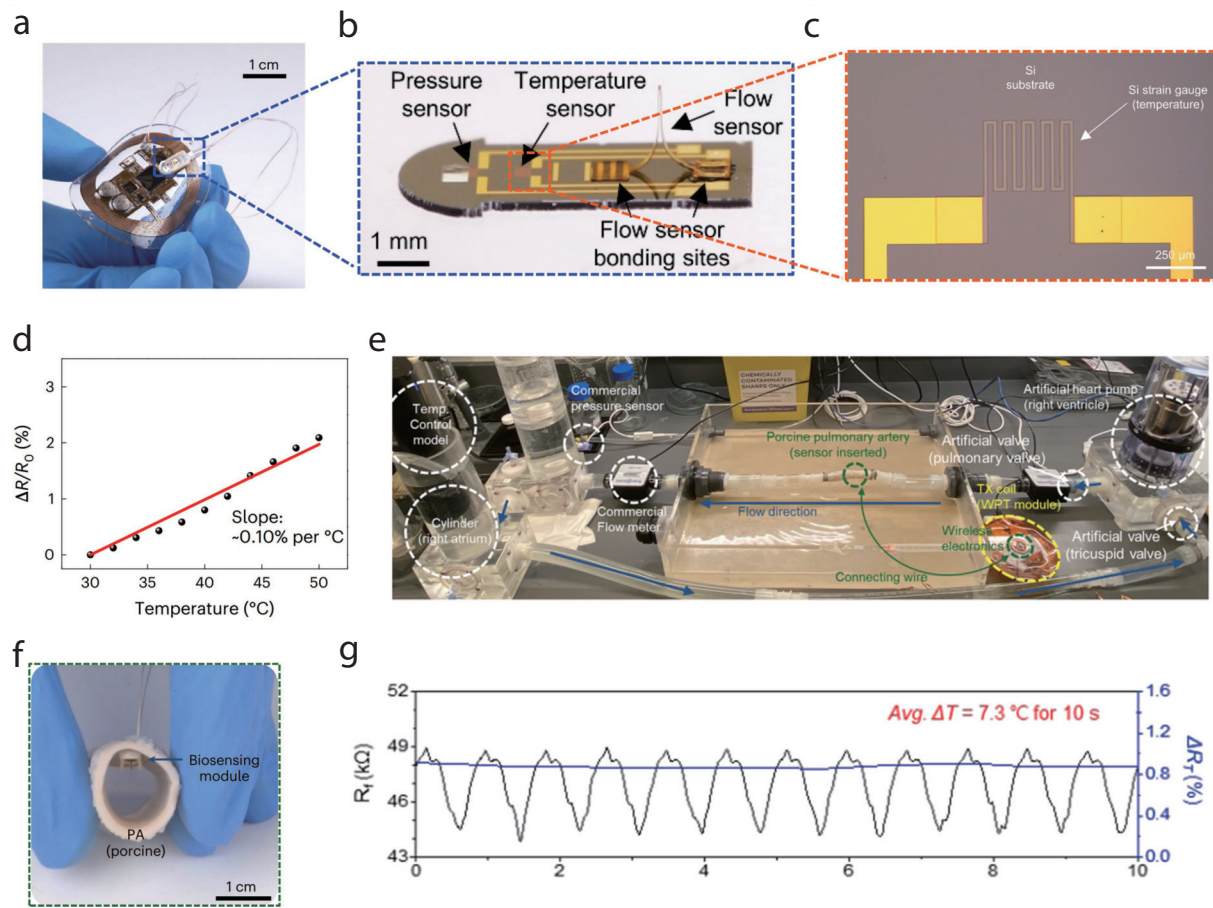


Fig. 4. (Color online) Biocompatible, battery-less wireless implantable temperature sensor based on silicon nanomembrane (Si-NM). (a) Optical image of the soft, flexible wireless electronics module interconnected with the biosensing module via insulated, flexible fine wires (blue dotted box). (b) Optical images of biosensing modules with pressure, temperature, and flow sensors. (c) Silicon serpentine strain gauges on a flat substrate for temperature monitoring. (d) Measured resistance change ($\Delta R/R_0$) response of approximately 0.10% $^{\circ}\text{C}^{-1}$ in the temperature sensor when exposed to temperature changes from 30 to 50 $^{\circ}\text{C}$. (e) Optical image of the artificial heart system, including two cylinders with mechanical pumps simulating the right ventricle (RV) and right atrium (RA), two prosthetic heart valves mimicking the pulmonary valve (PV) and tricuspid valve (TV), a temperature control module, and commercial sensors. (f) Optical image of the sensing module inserted into the pulmonary arteries (PA) extracted from a pig. (g) Simultaneous measurements of flow sensor resistance (R_f, black) and normalized resistance change of the temperature sensor (ΔR_T , blue) using the artificial heart system. Reproduced with permission from Ref. [41]. Copyright (2023) Nature Publishing Group.

tional element for various implantable sensors due to its mature manufacturing processes and excellent electrical characteristics. Due to their unique optical properties, other inorganic semiconductor materials like gallium arsenide (GaAs) are also becoming research focal points.

Kwon *et al.* have designed and validated an integrated wireless sensor system that comprises a battery-free wireless sensing module and an external wireless power transmission system^[41]. The sensing module utilizes single-crystalline silicon nanomembranes (Si-NMs) as the foundational material to measure blood flow velocity, pressure, and temperature. Figs. 4(a) and 4(b) present this implantable sensing utilizes a coil to eliminate the reliance on batteries in traditional devices and achieves long-distance data transmission through Bluetooth low energy (BLE) communication, ensuring real-time monitoring in postoperative care. Fig. 4(c) demonstrates the use of thin-layer serpentine single-crystalline silicon nanomembrane sensors in the sensing component for precise temperature monitoring. The temperature sensor measures 380 μm wide, 300 μm long, and 200 nm thick, based on a multilayer polyimide (PI) and Si-NM structure, facilitating easy integration into vascular or cardiac implant sites. Its opera-

tion relies on resistance changes that vary linearly with temperature changes, expressed as $\Delta R/R_0$ (where R_0 is the initial resistance value). Fig. 4(d) shows that the temperature sensor exhibits a highly linear response, with approximately 0.10% change per $^{\circ}\text{C}$ over the range of 30 to 50 $^{\circ}\text{C}$, while its resistance remains unaffected by pressure and other factors. Fig. 4(e) demonstrates the sensor system validated in a porcine pulmonary artery model and an artificial heart model, which includes two cylinders with mechanical pumps simulating the right ventricle (RV) and right atrium (RA), as well as two prosthetic heart valves mimicking the pulmonary valve (PV) and tricuspid valve (TV). Blood flow into the pulmonary artery (PA) is induced through a bileaflet mechanical valve that replicates the mechanical function of the PV. Fig. 4(f) shows the implanted sensor system within the PA and conducting a 10-s experiment using the artificial heart system to simulate physiological conditions while recording resistance changes in the flow sensor (R_f) and normalized resistance changes in the temperature sensor (ΔR_T). Fig. 4(g) highlights the exceptional sensitivity and stability of the temperature sensor. In the pulmonary artery model, the sensing module successfully measured blood flow while simultaneously record-

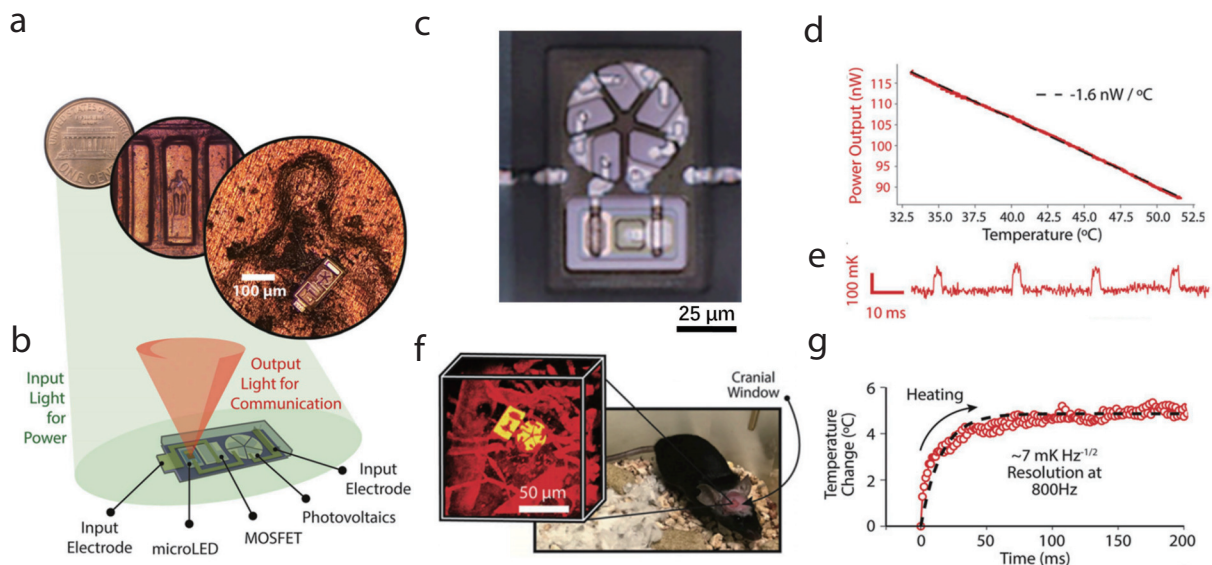


Fig. 5. (Color online) Implantable optical wireless integrated circuit temperature sensor based on silicon and III–V semiconductors. (a) Optical micrograph of a voltage-sensing optical wireless integrated circuit (OWIC) on the back of a penny. (b) Schematic of the OWIC in operation, illustrating the integration of optical communication, power, and electronics into a fully integrated microscopic sensor package. (c) Optical image of the setup used for temperature measurement of the OWIC sensor. (d) Graph depicting the characteristics of optical power output as a function of temperature. (e) Measurement of small, rapid temperature changes induced by a resistive element adjacent to the OWIC temperature sensor. (f) 3D reconstruction of the implanted OWIC and vasculature in a mouse brain, with blood vessels labeled using fluorescein and imaged via three-photon microscopy (1320 nm excitation, red), while the implanted OWIC is visualized through label-free third harmonic generation (yellow). (g) *In vivo* optical recording of temperature from the OWIC sensor, as input power heats the device and surrounding tissue. Reproduced with permission from Ref. [46]. Copyright (2020) National Academy of Sciences.

ing temperature, demonstrating reliable performance under these conditions. Additionally, the temperature sensor can calibrate other sensors to ensure the accuracy of blood flow and pressure measurements, especially with changes in ambient temperature. This wireless cardiac monitoring system is expected to play an increasingly significant role in clinical applications, demonstrating excellent performance in experiments by accurately capturing the pulsatile characteristics of temperature, pressure, and flow, thereby providing crucial support for diagnosing and treating cardiac diseases^[42, 43].

While implantable temperature sensors based on silicon nanomembranes (Si-NMs) have shown promise in biomedical applications, their size and wired connections limit their utility in certain microscale contexts. Researchers are exploring smaller, more flexible sensing platforms to advance micro-sensing technology^[44, 45]. In this context, the 100 μm scale temperature sensor developed by Cortese *et al.*^[46]. **Fig. 5(a)** illustrates a breakthrough with a 100 μm scale temperature sensor based on optically wireless integrated circuits (OWICs). This sensor achieves a size barely discernible to the naked eye and operates entirely wirelessly, opening new possibilities for microscale sensing and measurement. **Fig. 5(b)** shows that this platform combines silicon electronic devices and micro-LEDs for wireless optical communication and energy transfer. When exposed to light at a wavelength of 532 nm, a silicon photovoltaic cell powers the circuit, while an n-type metal–oxide–semiconductor (NMOS) device senses environmental signals, which are then output optical signals via micro-LEDs. **Fig. 5(c)** presents an optical image of the OWIC device designed for temperature detection, specifically showing the series structure of the Si photovoltaic cell in the circular area and the GaAs micro-LED underneath. **Fig. 5(d)** shows the relationship between the optical power output of

the OWIC and temperature change, indicating that the optical power output decreases linearly with increasing temperature. **Fig. 5(e)** demonstrates rapid temperature changes by placing a resistor near the OWIC for Joule heating and using the OWIC to record temperature changes in real-time. During this measurement, the OWIC achieved a temperature resolution of 3 mK-Hz^{-1/2} with a bandwidth of 1 kHz. **Fig. 5(f)** shows the *in vivo* experiments where a custom silicon microneedle was used to implant the OWIC 160 μm deep into a mouse brain and observed the OWIC and surrounding blood vessels using 3D imaging techniques, measuring an *in vivo* temperature resolution of 7 mK-Hz^{-1/2} with a response time of 10 ms, capable of monitoring rapid temperature changes up to 10³ K-s⁻¹ (**Fig. 5(g)**). This study demonstrates the significant potential of OWICs as micro-implantable sensors, offering an innovative solution for temperature monitoring in biomedicine. Further work is necessary to optimize OWIC manufacturing processes and address challenges related to biocompatibility, optical penetration depth, and application-specific issues. The miniature OWIC sensor platform exhibits exceptional sensitivity and precision in temperature measurement, making it suitable for microscale environments.

While the temperature-dependent photoluminescence (PL) mechanism via downconversion requires short-wavelength excitation, the upconversion process, converting near-infrared (NIR) photons within the biological transparency window (~650–950 nm) to visible photons, offers substantial advantages^[47–49]. This is particularly relevant for biomedical applications, as NIR light penetrates tissue better and reduces interference from biological autofluorescence^[50]. Ding *et al.* have developed a temperature sensor based on this upconversion process, demonstrating a linear response and ultra-fast

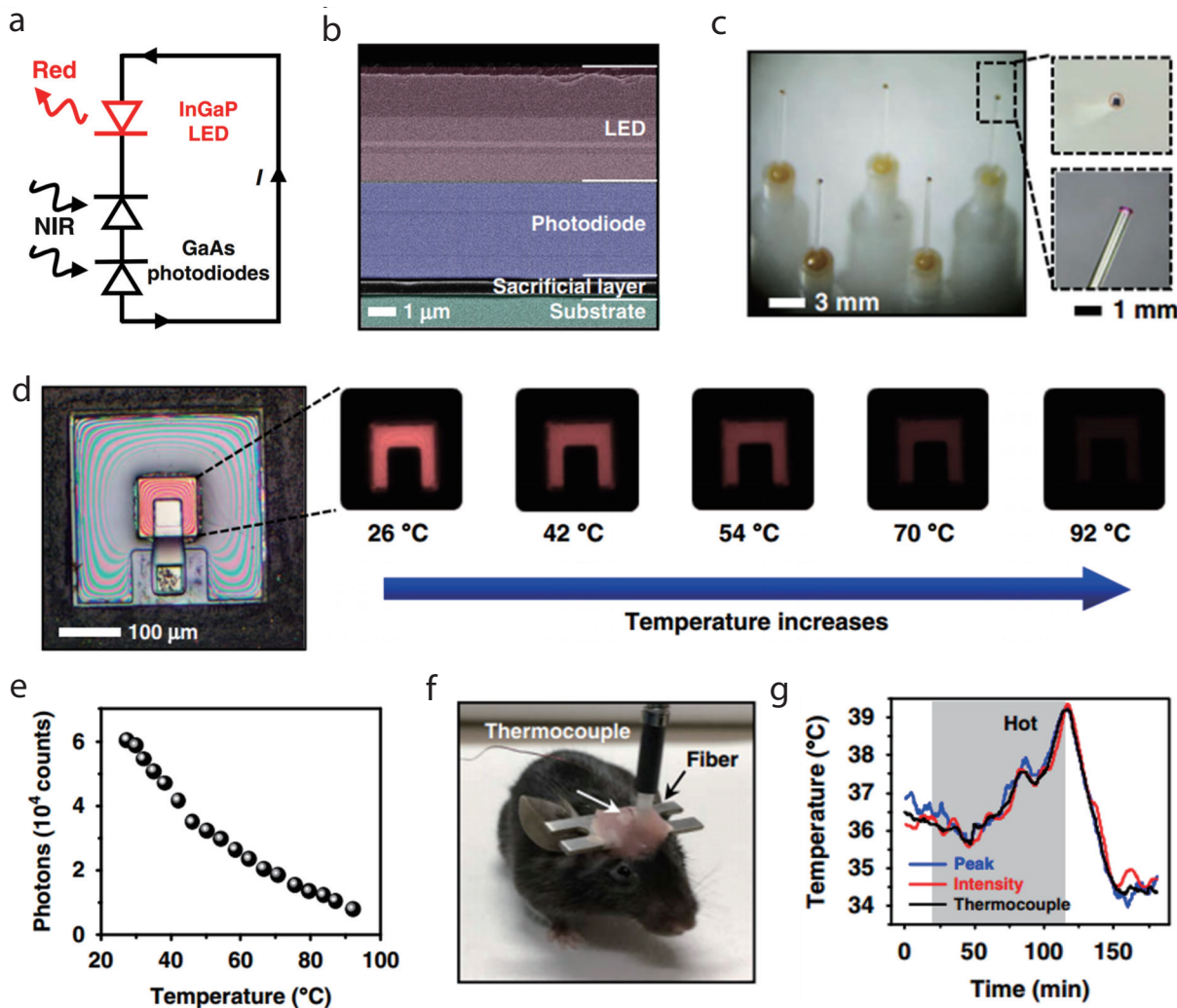


Fig. 6. (Color online) Implantable optoelectronic upconversion temperature sensor based on III–V semiconductors. (a) Circuit schematic diagram of the optoelectronic temperature sensor, featuring an InGaP red LED and a GaAs double junction photodiode connected in series. (b) Scanning electron microscopy (SEM) image detailing the design of the optoelectronic upconversion device. (c) Optical image of upconversion devices transferred onto the tips of fibers (diameter approximately $600 \mu\text{m}$), with insets providing a zoomed-in view of the fiber tips with a red-emitting device excited by coupled near-infrared light. (d) Microscopic top view of an upconversion device for temperature sensing under infrared excitation, along with photoluminescence (PL) emissions of the device as temperature varies from 26 to 92 °C. (e) Relationship between PL intensity and temperature, measured by counting the average number of captured photons with an imaging sensor. (f) Optical image of a mouse with an implanted fiber sensor and thermocouple in the brain for temperature sensing. (g) Dynamic temperature signals obtained in the mouse brain compared to results recorded simultaneously with thermocouples, with the shaded gray region indicating when the mouse was placed in a hot environment (~ 40 °C). Reproduced with permission from [51]. Copyright (2022) Nature Publishing Group.

dynamic characteristics that enable real-time monitoring of temperature fluctuations in complex biological environments^[51]. As shown in Fig. 6(a), this device consists of a low-bandgap gallium arsenide (GaAs) double-junction photodiode connected in series with a wide-bandgap indium gallium phosphide (InGaP) light-emitting diode (LED). Fig. 6(b) presents a cross-sectional scanning electron microscopy (SEM) image of the device structure with a size of $\sim 300 \mu\text{m} \times 300 \mu\text{m}$ on a GaAs substrate and a sacrificial intermediate layer. Fig. 6(c) illustrates the integration of the freestanding thin-film optoelectronic upconversion device on the tip of a quartz optical fiber. The magnified image shows the red light-emitting device at the fiber tip, which emits visible light when irradiated with NIR light. Figs. 6(d) and 6(e) present the luminescence performance of this optoelectronic upconversion device over a temperature range of 26 to 92 °C, showing that as temperature increases, the PL intensity signifi-

cantly decreases. Fig. 6(e) further quantifies the relationship between PL intensity (measured by the average number of photons captured by the imaging sensor) and temperature, indicating a linear decrease in luminescence intensity with temperature, confirming the capability for precise temperature detection under various thermal conditions. Figs. 6(f) and 6(g) demonstrate the application of this integrated optoelectronic upconversion device in deep brain temperature monitoring *in vivo*. The graphs show brain temperature changes recorded simultaneously by the fiber optic sensor and a thermocouple over time. The results indicate a significant rise in brain temperature when the experimental mouse is placed in a high-temperature environment (~ 40 °C), with a corresponding decline as ambient temperature decreases. The temperature measured by the fiber optic sensor is highly consistent with the thermocouple measurements, with an absolute coefficient (R^2) of temperature change recorded by both sensors

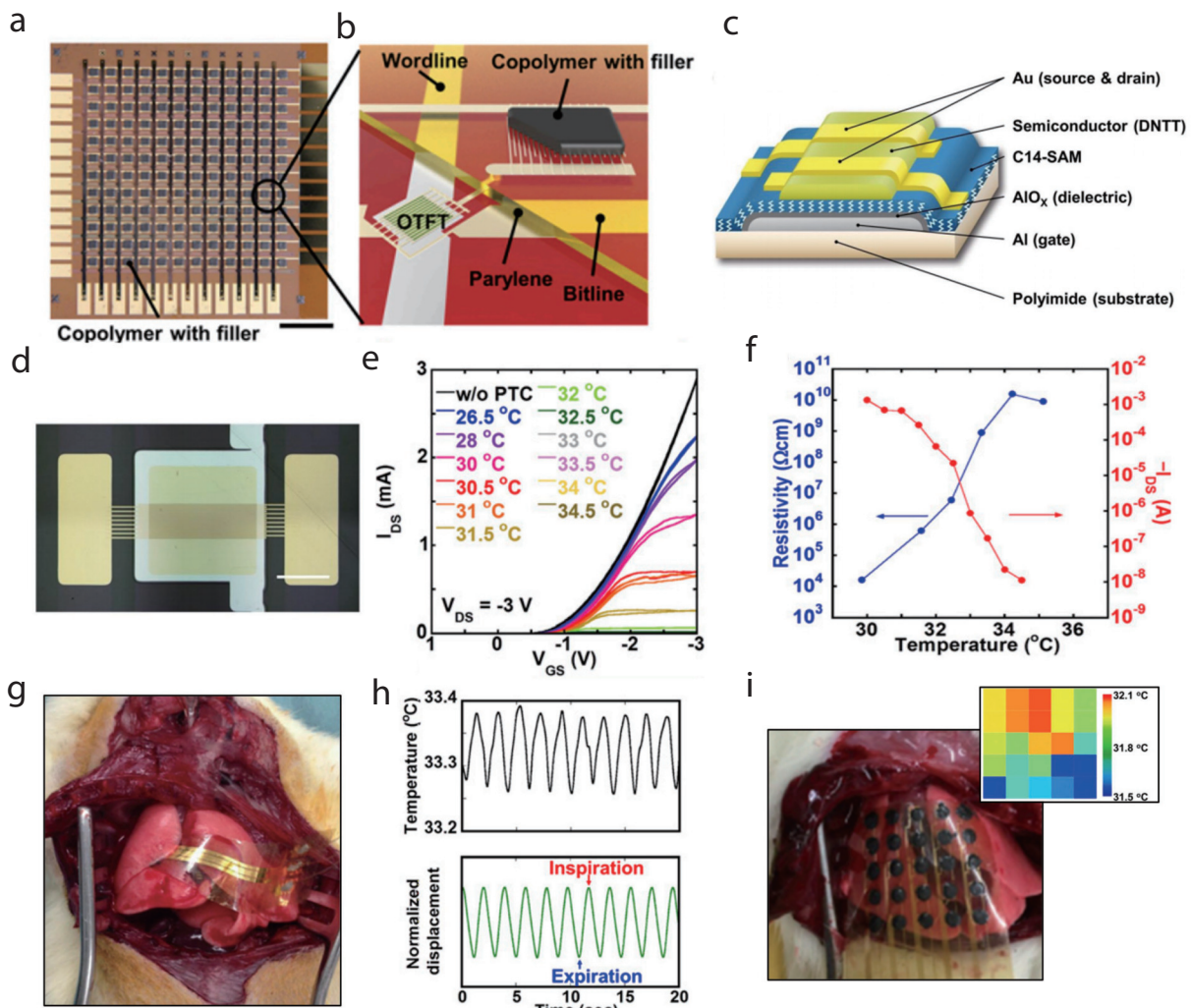


Fig. 7. (Color online) Implantable physiological temperature sensor for organic semiconductor-based materials. (a) Image of a flexible 12 × 12 temperature sensor sheet (scale bar: 1 cm). (b) Cross-sectional illustration of a flexible large-area active-matrix sensor array with 12 × 12 temperature pixels. (c) Structure of the organic transistor, featuring a gate dielectric made of an anodized aluminum oxide layer and a phosphonic acid self-assembled monolayer (SAM); a 30 nm thick layer of dinaphtho[2,3-b:2',3'-f]thieno[3,2-b]thiophene (DNTT) serves as the air-stable organic semiconductor forming the channel layer. (d) Optical image of the organic transistor. (e) Temperature dependence of the electrical characteristics after integrating the temperature sensor with the organic transistor. (f) Temperature dependence of the resistivity of the temperature sensor and the on-current of the organic transistor with the integrated temperature sensor. (g) Temperature measurement of respiratory lung tissue, illustrating heat exchange between the lung tissue and air. (h) Time course of the living lung's temperature (black: temperature output from the sensor, green: displacement of the lung surface). (i) Temperature mapping measurement of a rat lung using a 5 × 5 array of temperature sensors. Reproduced with permission from Ref. [55]. Copyright (2015) National Academy of Sciences.

exceeding 0.97. The unique technological aspect of this device lies in its integrated fabrication process for both light reception and emission components, combining the advantages of upconversion technology to achieve microscale, implantable temperature monitoring. This approach enhances device reliability and stability, laying the foundation for large-scale production and cost control. By integrating optical fiber technology, researchers have demonstrated potential applications in human respiration monitoring and deep brain temperature detection in animals. This technology also exhibits advantages in MRI compatibility^[52], particularly for deep brain temperature monitoring, providing a novel tool for neuroscience research.

4. Organic semiconductor-based implantable temperature sensor

Organic semiconductor materials offer several advan-

tages over inorganic options, particularly in processing and manufacturing. They can be produced using low-cost, large-area techniques that meet the design requirements of sensor devices, providing comfort and flexibility for continuous physiological monitoring^[53, 54]. These traits make organic semiconductors ideal for developing flexible and stretchable sensors. However, their stability and performance pose challenges for implantable uses.

Yokota *et al.* have developed a flexible and sensitive temperature sensor made from a composite of semi-crystalline acrylate polymer and graphite^[55]. Fig. 7(a) showcases an ultra-flexible temperature sensor array, while Fig. 7(b) illustrates the cross-sectional structure of the sensor, consisting of multiple temperature-sensing units arranged in a 12 × 12 organic active matrix, totaling 144 temperature-sensing pixels. This sensor array is built on a thin, flexible substrate that conforms to curved surfaces, making it suitable for tempera-

Table 1. Comparison of parameters for representative of temperature sensors.

Materials	Size (μm)	TCR/Sensitivity ($^{\circ}\text{C}^{-1}$)	Time response (ms)	Temperature range ($^{\circ}\text{C}$)	Manufacturing difficulty	Cost	Yield	Ref
Au	$\sim 150 \times 150$	0.32%	1300	18–41	Easy	Medium	Low	[25]
Au	$\sim 800 \times 800$ (one pixel)	0.17%	~ 25	30–80	Complex	Medium	Low	[30]
Mn–Co–Ni–O	$210 \times 180 \times 4.1$	4 %	224	25–100	Medium	Low	Medium	[38]
Si-nm	$\sim 375 \times 315$	0.1%	—	30–50	Complex	Medium	Low	[41]
Si and III–V semiconductors	$380 \times 300 \times 0.2$	2 %	10	20–40	Complex	High	High	[46]
III–V semiconductors	300×300	1.5 %	~ 0.02	25–90	Medium	High	High	[51]
Dinaphtho[2,3-b:29,39-f]thieno[3,2-b]thiophene (DNTT)	38.5 (thick)	Resistance changes by 6 orders of magnitude within 5 °C	<100	25–50 (require tune)	Easy	Low	Medium	[55]

ture measurements on dynamic surfaces such as the human body. The core of this sensor system is its organic transistor structure (Figs. 7(c) and 7(d)). The transistor gate electrode consists of a 100 nm thick aluminum layer covered with aluminum oxide that serves as the gate dielectric. This aluminum oxide layer, formed through anodic oxidation, is enhanced with a self-assembled monolayer (SAM) of phosphonic acid to improve the interface between the organic semiconductor and the gate dielectric. The transistor channel layer uses a 30 nm thick air-stable organic semiconductor, DNTT, with gold electrodes serving as the source and drain. Fig. 7(e) depicts the relationship between the electrical characteristics of the temperature sensor integrated with the organic transistor and temperature changes. As the temperature increases, the resistance of the sensor rises, resulting in a decrease in the drain current of the organic transistor. Fig. 7(f) illustrates that as the temperature increases from 30.0 to 34.5 °C, the drain current drops from 1 mA to 10 nA, achieving a change of over 10^5 times in magnitude and demonstrating high resolution in temperature detection. To evaluate the potential in biomedical applications, the sensor is placed directly on a rat lung to monitor temperature changes during respiration (Fig. 7(g)). Fig. 7(h) shows the results of the sensor effectively capturing periodic temperature fluctuations caused by breathing, with a variation range of approximately 0.1 °C. The researchers also monitored lung surface displacement, confirming that the observed temperature variations were caused by respiration rather than external factors. Fig. 7(i) further illustrates the capability of thermal imaging of the rat lung using a 5×5 temperature sensor array. These experiments highlight the potential of this novel sensor in advanced medical diagnostics and monitoring applications. This research offers exceptional sensitivity, significantly simplifying the data read-out circuitry, and opening new avenues for physiological monitoring and medical diagnostics. However, compared to metal resistance temperature sensors, the temperature response of this organic sensor is less linear, and its measurement range remains relatively limited.

5. Conclusion and perspective

In summary, implantable temperature sensors rapidly transform medical research and change how we monitor and understand physiological states. We have reviewed the latest

advances in this field, focusing on applying different materials. Metal-based, inorganic, and organic semiconductor materials are the three main research directions for implantable temperature sensors, each with unique advantages and challenges. Table 1 summarizes the key performance parameters of implantable temperature sensors based on different material types. While metal-based materials may not excel in certain parameters compared to others, their stability and reliability make them suitable for long-term implantation monitoring. These small-footprint temperature sensors benefit from established microfabrication, which contributes to cost-effective production [56]. Inorganic semiconductor materials, particularly silicon-based sensors, excel in resolution and response time but require relatively complex microfabrication techniques that increase manufacturing costs [57]. In contrast, organic semiconductor materials offer high sensitivity and various options, making them ideal for precision biomedical monitoring. They can be processed using low-cost techniques, such as printing and coating, allowing for flexible and stretchable designs [58, 59]. These characteristics serve as a significant reference for the future design and optimization of temperature sensors.

Continuous advancements in materials science and manufacturing technologies will enhance the functionality, performance, and application possibilities of implantable temperature sensors. Future research should prioritize biocompatibility, long-term stability, multifunctional integration, intelligence, wireless power supply, and communication systems. These improvements are crucial for optimal sensor performance in complex physiological environments. Biocompatibility is a crucial consideration in the development of implantable temperature sensors, as it ensures their safe and effective functionality within the human body. This biocompatibility can be improved by applying protective coatings and selecting materials carefully. Coatings such as parylene and medical-grade silicone serve to isolate the sensors from surrounding tissues, thereby mitigating immune responses and inflammation while enhancing corrosion resistance and overall stability [60, 61]. Recently developed coatings, including hyaluronic acid/gelatin nanocomposite hydrogel coatings, inhibit inflammatory responses and protect normal tissues [62]. In terms of materials, gold (Au) and platinum (Pt) are favored for their inherent stability and low reactivity [63], while silicon-

based materials frequently undergo surface treatments to improve their biocompatibility^[64]. Moreover, the emergence of organic semiconductor materials introduces increased flexibility and reduces tissue irritation, making them particularly suitable for use in implantable devices^[65]. Innovations in miniaturization and wireless will expand the use of these sensors in telemedicine and dynamic physiological monitoring. Implantable temperature sensors are becoming essential for precision medicine, offering personalized treatment options and intelligent health management. These sensors can potentially transform clinical diagnosis, surgical assistance, and life science research. As the field progresses, the focus is on overcoming challenges to develop more precise, reliable, and multi-functional implantable temperature sensor systems. Such advancements are expected to significantly contribute to human health, ushering in a new era of biomedical technology.

Acknowledgments

This work is supported by the National Natural Science Foundation of China (NSFC) (62422501), Beijing Nova Program (20230484254, 20240484742), and Hebei Natural Science Foundation (F2024105039).

References

- [1] Koydemir H C, Ozcan A. Wearable and implantable sensors for biomedical applications. *Annual Rev Anal Chem*, 2018, 11, 127
- [2] Pang C, Lee C, Suh K Y. Recent advances in flexible sensors for wearable and implantable devices. *J Appl Polym Sci*, 2013, 130, 1429
- [3] Kiyatkin E A, Brown P L, Wise R A. Brain temperature fluctuation: A reflection of functional neural activation. *Eur J Neurosci*, 2002, 16, 164
- [4] Sim D, Brothers M C, Slocik J M, et al. Biomarkers and detection platforms for human health and performance monitoring: A review. *Adv Sci*, 2022, 9, 2104426
- [5] Cramer M N, Gagnon D, Laitano O, et al. Human temperature regulation under heat stress in health, disease, and injury. *Physiol Rev*, 2022, 102, 1907
- [6] Niedermann R, Wyss E, Annaheim S, et al. Prediction of human core body temperature using non-invasive measurement methods. *Int J Biometeorol*, 2014, 58, 7
- [7] Lahiri B B, Bagavathiappan S, Jayakumar T, et al. Medical applications of infrared thermography: A review. *Infrared Phys Technol*, 2012, 55, 221
- [8] Singh R, Bathaei M J, Istif E, et al. A review of bioresorbable implantable medical devices: Materials, fabrication, and implementation. *Adv Healthcare Mater*, 2020, 9, 2000790
- [9] Ashammakhi N, Hernandez A L, Unluturk B D, et al. Biodegradable implantable sensors: Materials design, fabrication, and applications. *Adv Funct Mater*, 2021, 31, 2104149
- [10] Lu D, Yan Y, Avila R, et al. Bioresorbable, wireless, passive sensors as temporary implants for monitoring regional body temperature. *Adv Healthcare Mater*, 2020, 9, 2000942
- [11] Dakurah M N, Koo C, Choi W, et al. Implantable bladder sensors: A methodological review. *Int Neurourol J*, 2015, 19, 133
- [12] Scholten K, Meng E. Materials for microfabricated implantable devices: A review. *Lab Chip*, 2015, 15, 4256
- [13] Koo J H, Song J K, Yoo S, et al. Unconventional device and material approaches for monolithic biointegration of implantable sensors and wearable electronics. *Adv Mater Technol*, 2020, 5, 2000407
- [14] Yang T, Deng W L, Chu X, et al. Hierarchically microstructure-
bioinspired flexible piezoresistive bioelectronics. *ACS Nano*, 2021, 15, 11555
- [15] Qin Y, Mo J L, Liu Y H, et al. Stretchable triboelectric self-powered sweat sensor fabricated from self-healing nanocellulose hydrogels. *Adv Funct Mater*, 2022, 32, 2201846
- [16] He M, Du W W, Feng Y M, et al. Flexible and stretchable triboelectric nanogenerator fabric for biomechanical energy harvesting and self-powered dual-mode human motion monitoring. *Nano Energy*, 2021, 86, 106058
- [17] Andreu-Perez J, Leff D R, Ip H M D, et al. From wearable sensors to smart implants—toward pervasive and personalized healthcare. *IEEE Trans Biomed Eng*, 2015, 62, 2750
- [18] Liu Y Q, Yu Q, Yang L, et al. Materials and biomedical applications of implantable electronic devices. *Adv Mater Technol*, 2023, 8, 2200853
- [19] Liu Z J, Tian B, Fan X, et al. A temperature sensor based on flexible substrate with ultra-high sensitivity for low temperature measurement. *Sens Actuat A Phys*, 2020, 315, 112341
- [20] Mailly F, Giani A, Bonnot R, et al. Anemometer with hot platinum thin film. *Sens Actuat A Phys*, 2001, 94, 32
- [21] Ali M S, Ali M S, Mallick S, et al. Dual parameter smart sensor for nitrogen and temperature sensing based on defect-engineered 1T-MoS₂. *Sci Rep*, 2024, 14, 21469
- [22] Sun X, Li Z C, Fu W Y, et al. Li/Fe modified Zn_{0.3}Ni_{0.7}O NTC thermistors with adjustable resistivities and temperature sensitivity. *J Mater Sci Mater Electron*, 2018, 29, 343
- [23] Paladiya C, Kiani A. Nano structured sensing surface: Significance in sensor fabrication. *Sens Actuat B Chem*, 2018, 268, 494
- [24] Chatterjee S, Saxena M, Padmanabhan D, et al. Futuristic medical implants using bioresorbable materials and devices. *Biosens Bioelectron*, 2019, 142, 111489
- [25] Wang J Q, Xie H, Chung T, et al. Neural probes with integrated temperature sensors for monitoring retina and brain implantation and stimulation. *IEEE Trans Neural Syst Rehabil Eng*, 2017, 25, 1663
- [26] Moser Y, Gijs M A M. Miniaturized flexible temperature sensor. *J Microelectromech Syst*, 2007, 16, 1349
- [27] Xiao S Y, Che L F, Li X X, et al. A novel fabrication process of MEMS devices on polyimide flexible substrates. *Microelectron Eng*, 2008, 85, 452
- [28] Li Q, Zhang L N, Tao X M, et al. Review of flexible temperature sensing networks for wearable physiological monitoring. *Adv Healthcare Mater*, 2017, 6, 1601371
- [29] Shao Z C, Pala S, Liang Y, et al. Non-contact surface temperature sensing based on a single bimorph pMUTS array. 2020 IEEE 33rd International Conference on Micro Electro Mechanical Systems (MEMS), 2020, 861
- [30] Han M D, Chen L, Aras K, et al. Catheter-integrated soft multilayer electronic arrays for multiplexed sensing and actuation during cardiac surgery. *Nat Biomed Eng*, 2020, 4, 997
- [31] Kim D H, Lu N S, Ghaffari R, et al. Materials for multifunctional balloon catheters with capabilities in cardiac electrophysiological mapping and ablation therapy. *Nat Mater*, 2011, 10, 316
- [32] Lee S P, Klinker L E, Ptaszek L, et al. Catheter-based systems with integrated stretchable sensors and conductors in cardiac electrophysiology. *Proc IEEE*, 2015, 103, 682
- [33] Kim Y, Parada G A, Liu S D, et al. Ferromagnetic soft continuum robots. *Sci Robot*, 2019, 4, eaax7329
- [34] Yokota T, Zalar P, Kaltenbrunner M, et al. Ultraflexible organic photonic skin. *Sci Adv*, 2016, 2, e1501856
- [35] Arndt-Jovin D J, Robert-Nicoud M, Kaufman S J, et al. Fluorescence digital imaging microscopy in cell biology. *Science*, 1985, 230, 247
- [36] Cho M, Han J K, Suh J, et al. Fully bioresorbable hybrid opto-electronic neural implant system for simultaneous electrophysiological recording and optogenetic stimulation. *Nat Commun*, 2024,

- 15, 2000
- [37] Jiang N, Chang X H, Hu D W, et al. Flexible, transparent, and anti-bacterial ionogels toward highly sensitive strain and temperature sensors. *Chem Eng J*, 2021, 424, 130418
- [38] Cui Y Y, Sun M W, Liu C B, et al. All-inorganic ultrathin high-sensitivity transparent temperature sensor based on a Mn–Co–Ni–O nanofilm. *Microsyst Nanoeng*, 2024, 10, 70
- [39] Yu K J, Yan Z, Han M D, et al. Inorganic semiconducting materials for flexible and stretchable electronics. *NPJ Flex Electron*, 2017, 1, 4
- [40] Liu G, Lv Z Y, Batool S, et al. Biocompatible material-based flexible biosensors: From materials design to wearable/implantable devices and integrated sensing systems. *Small*, 2023, 19, 2207879
- [41] Kwon K, Kim J U, Won S M, et al. A battery-less wireless implant for the continuous monitoring of vascular pressure, flow rate and temperature. *Nat Biomed Eng*, 2023, 7, 1215
- [42] Milani-Nejad N, Janssen P M L. Small and large animal models in cardiac contraction research: Advantages and disadvantages. *Pharmacol Ther*, 2014, 141, 235
- [43] Camacho P, Fan H M, Liu Z M, et al. Small mammalian animal models of heart disease. *Am J Cardiovasc Dis*, 2016, 6, 70
- [44] Charthad J, Weber M J, Chang T C, et al. A mm-sized implantable medical device (IMD) with ultrasonic power transfer and a hybrid bi-directional data link. *IEEE J Solid State Circuits*, 2015, 50, 1741
- [45] Lee S, Cortese A J, Gandhi A P, et al. A $250\text{ }\mu\text{m} \times 57\text{ }\mu\text{m}$ micro-scale opto-electronically transduced electrodes (MOTES) for neural recording. *IEEE Trans Biomed Circuits Syst*, 2018, 12, 1256
- [46] Cortese A J, Smart C L, Wang T Y, et al. Microscopic sensors using optical wireless integrated circuits. *Proc Natl Acad Sci USA*, 2020, 117, 9173
- [47] Xu M, Zou X M, Su Q Q, et al. Ratiometric nanothermometer in vivo based on triplet sensitized upconversion. *Nat Commun*, 2018, 9, 2698
- [48] Chen G Y, Qiu H L, Prasad P N, et al. Upconversion nanoparticles: Design, nanochemistry, and applications in theranostics. *Chem Rev*, 2014, 114, 5161
- [49] Chernov M V, Gushchin S V, Kuzmin A M, et al. Infrared to visible up-conversion luminescence of SrF_2 : Ho particles upon excitation of the 5I7 level of Ho^{3+} ions. *J Lumin*, 2023, 261, 119942
- [50] Lee G H, Moon H, Kim H, et al. Multifunctional materials for implantable and wearable photonic healthcare devices. *Nat Rev Mater*, 2020, 5, 149
- [51] Ding H, Lv G Q, Cai X, et al. An Optoelectronic thermometer based on microscale infrared-to-visible conversion devices. *Light Sci Appl*, 2022, 11, 130
- [52] Shin J, Liu Z H, Bai W B, et al. Bioresorbable optical sensor systems for monitoring of intracranial pressure and temperature. *Sci Adv*, 2019, 5, eaaw1899
- [53] Zhu C X, Wu H C, Nyikayaramba G, et al. Intrinsically stretchable temperature sensor based on organic thin-film transistors. *IEEE Electron Device Lett*, 2019, 40, 1630
- [54] Someya T, Bao Z N, Malliaras G G. The rise of plastic bioelectronics. *Nature*, 2016, 540, 379
- [55] Yokota T, Inoue Y, Terakawa Y, et al. Ultraflexible, large-area, physiological temperature sensors for multipoint measurements. *Proc Natl Acad Sci USA*, 2015, 112, 14533
- [56] Chen Y, Pépin A. Nanofabrication: Conventional and nonconventional methods. *Electrophoresis*, 2001, 22, 187
- [57] Mittal M, Sardar S, Jana A. Nanofabrication techniques for semi-conductor chemical sensors. *Handbook of Nanomaterials for Sensing Applications*. Amsterdam: Elsevier, 2021, 119
- [58] Ahmad S. Organic semiconductors for device applications: Current trends and future prospects. *J Polym Eng*, 2014, 34, 279
- [59] Eslamian M. Inorganic and organic solution-processed thin film devices. *Nanomicro Lett*, 2017, 9, 3
- [60] Vishwakarma A, Bhise N S, Evangelista M B, et al. Engineering immunomodulatory biomaterials to tune the inflammatory response. *Trends Biotechnol*, 2016, 34, 470
- [61] Zhang D H, Chen Q, Shi C, et al. Dealing with the foreign-body response to implanted biomaterials: Strategies and applications of new materials. *Adv Funct Mater*, 2021, 31, 2007226
- [62] Ding Y, Ma R C, Liu G H, et al. Fabrication of a new hyaluronic acid/gelatin nanocomposite hydrogel coating on titanium-based implants for treating biofilm infection and excessive inflammatory response. *ACS Appl Mater Interfaces*, 2023, 15, 13783
- [63] Basova T V, Vikulova E S, Dorovskikh S I, et al. The use of noble metal coatings and nanoparticles for the modification of medical implant materials. *Mater Des*, 2021, 204, 109672
- [64] Kros A, Gerritsen M, Sprakel V S I, et al. Silica-based hybrid materials as biocompatible coatings for glucose sensors. *Sens Actuat B Chem*, 2001, 81, 68
- [65] Chen K, Ren J Y, Chen C Y, et al. Safety and effectiveness evaluation of flexible electronic materials for next generation wearable and implantable medical devices. *Nano Today*, 2020, 35, 100939

Zhuofan Yang received his BS degree from Beijing Forestry University in 2020. He is now a postgraduate student of Beijing Institute of Technology, under the guidance of Professor He Ding.



Hongcheng Song received his Ph.D. from Capital Medical University, Beijing, China, in 2012. He pursued advanced studies in urology at Morgan Stanley Children's Hospital of New York and Children's Hospital Los Angeles in 2014. He is currently a chief physician at Beijing Children's Hospital and an Associate Professor at Capital Medical University.



He Ding received his Ph.D. from Ecole Centrale de Lyon, France, in 2016 and postdoctoral studies at Tsinghua University, Beijing, China, from 2016 to 2018. He is currently an Associate Professor at the School of Optics and Photonics, Beijing Institute of Technology, Beijing.

